Veterinary Medicine and Science

WILEY

ORIGINAL ARTICLE OPEN ACCESS

Exotics

Cadaveric Study of the Juvenile Grey Heron's (*Ardea cinerea*) Nasal Cavity and Associated Structures Through Computed Tomography and Anatomical Sections

Natalia Roldán-Medina[1] | Pablo Paz-Oliva[1] | Álvaro Ros[1] | Carlos Melián[2,3] | Esteban Pérez[2,3] | Alejandro Morales-Espino[4] | Manuel Morales[2] | Francisco Suárez-Cabrera[1] | José Raduan Jaber[1,3]

[1]Department of Morphology, Faculty of Veterinary Medicine, University of Las Palmas de Gran Canaria, Gran Canaria, Spain | [2]Department of Animal Pathology, Animal Production, Food Science and Technology, Faculty of Veterinary Medicine, University of Las Palmas de Gran Canaria, Gran Canaria, Spain | [3]VETFUN, Grupo de Innovación Educativa, University of Las Palmas de Gran Canaria, Gran Canaria, Spain | [4]IVC Evidensia Los Tarahales, Gran Canaria, Spain

Correspondence: José Raduan Jaber (joseraduan.jaber@ulpgc.es)

Received: 2 July 2025 | **Revised:** 19 March 2026 | **Accepted:** 13 April 2026

Keywords: anatomical cross-sections | anatomy | computed tomography | grey heron | head | nasal cavity

ABSTRACT

Background: The grey heron (*Ardea cinerea*) is a large wading bird whose cranial anatomy reflects its piscivorous habits and aquatic lifestyle. The nasal cavity plays a key role in respiratory function and represents an important structure in the diagnosis and management of upper respiratory diseases. However, detailed anatomical descriptions integrating gross anatomy and advanced imaging remain limited for this species.

Methods: Three juvenile grey heron cadavers underwent transverse computed tomography (CT) scanning, followed by corresponding anatomical cross-sectioning. This combined approach enabled precise correlation of bony structures, soft tissues, and sinus components.

Results: CT imaging allowed clear identification of the rostral, middle, and caudal nasal conchae; the infraorbital sinus and its rostral diverticulum; the nasal septum and septal sinus; and the elongated choanal cleft, which differed from patterns described in terrestrial birds. Anatomical sections provided additional detail regarding the spatial relationships between conchae, meatuses, and surrounding bones, and confirmed the presence of a small, poorly developed nasal gland. Three-dimensional reconstructions further enhanced spatial understanding of the nasal cavity and associated cranial structures.

Conclusions: This study establishes the first integrated anatomical and CT-based reference for the nasal cavity in the grey heron. The findings improve the interpretation of diagnostic imaging and provide a valuable framework for the evaluation of sinonasal and orbital disorders in aquatic avian species.

1 | Introduction

The grey heron (*Ardea cinerea*), distinguishes itself as an iconic species in the world of aquatic birds. It can be found throughout Europe, Asia, and Africa, frequenting several environments, such as woodland, urban and suburban, marine and intertidal, farmland, wetland and grassland (Boisteau and Marion 2007; Garrido et al. 2011; Cardarelli et al. 2017). There are no remarkable differences between female and male individuals, other than the male being somewhat larger (Garrido et al. 2011). This widespread wading bird is frequently admitted to rehabilitation centres with traumatic, metabolic, infectious or environmentally related

conditions (Montesdeoca et al. 2017). Although the species has been well described from a biological and behavioural standpoint (Boisteau and Marion 2007; Garrido et al. 2011; Cardarelli et al. 2017), its cranial and upper respiratory anatomy remains poorly documented. This limitation is relevant because the nasal cavity plays essential roles in thermoregulation, filtration, olfaction, and conditioning of inhaled air (Geist 2000; Casteleyn et al. 2018; Mahmoud et al. 2018), and disorders of this region are frequently encountered in aquatic birds.

Despite the clinical relevance of the avian upper respiratory tract, detailed anatomical descriptions of the nasal cavity remain scarce for most aquatic and wading species. Existing knowledge derives mainly from domestic birds such as chickens and pigeons (King and McLelland 1984; Casteleyn et al. 2018), whereas the sinonasal anatomy of long-beaked, piscivorous birds has received comparatively little attention (Madkour 2019; Morales-Espino, Déniz, et al. 2024; Jaber et al. 2025). This gap limits the interpretation of diagnostic imaging in Ardeidae, where morphological adaptations—including an elongated beak and an extensive infraorbital sinus system—likely influence nasal architecture and disease presentation.

Radiography has historically been used to examine the avian nasal cavity (Gibbs et al. 1979; Schwarz et al. 2000; Wilson et al. 2014), but its utility is limited by superimposition of structures. By contrast, computed tomography (CT) provides superior sensitivity, accuracy, and three-dimensional characterization of the skull (Burk 1992; Arencibia et al. 2000; De Rycke et al. 2003; Orosz and Lichtenberger 2011; Bavdek et al. 2017). Although CT has been used to describe cranial anatomy in macaws, parrots, parakeets, ostriches, cockatiels and shearwaters (Veladiano et al. 2016; Bavdek et al. 2017; Aref et al. 2024; Morales-Espino, Déniz, et al. 2024; Kazemi et al. 2025), only a few studies have specifically examined the avian nasal cavity. Accurate interpretation requires species-specific anatomical references because the configuration of the nasal conchae, meatuses and infraorbital sinus varies widely across avian taxa.

Given these gaps, there is a clear need for a combined anatomical and CT-based description of the grey heron's nasal cavity. Such a reference would support diagnostic imaging and clinical management of sinonasal and orbital disease in aquatic avian species. This study provides the first integrated anatomical and computed tomographic characterization of the nasal cavity and associated structures in juvenile grey herons, establishing a foundational reference for clinicians, radiologists and researchers working with wading birds.

2 | Materials and Methods

2.1 | Animals

The present study was conducted on three juvenile grey heron (*A. cinerea*) carcasses to evaluate the main formations of their nasal cavity. The animals had an average weight of 1.05 kg (ranging from 0.8 to 1.3 kg) and an average size of 88.5 cm (ranging from 85 to 92 cm) from beak to tail base. These specimens were obtained from the Wildlife Rehabilitation Centre after natural death or euthanasia for reasons unrelated to the head or respiratory system. Only cadavers in good preservation condition, without evidence of craniofacial trauma or advanced post-mortem decomposition, were included. The number of specimens analyzed reflects the limited availability of suitable grey heron carcasses meeting the inclusion criteria obtained from wildlife rehabilitation centres. This type of sample size is consistent with previous anatomical and CT-based studies in wild avian species, where access to well-preserved specimens is often limited (Morales-Espino, Fumero-Hernández, et al. 2024; Jaber et al. 2025).

Although the exact post-mortem interval was not documented in hours, all specimens were promptly refrigerated after death and handled under appropriate conditions to preserve tissue integrity and ensure optimal image quality. Approximately 1 week after death, the carcasses were removed from the freezer and allowed to thaw under controlled conditions for 24 h prior to imaging, ensuring adequate thermal equilibration and minimizing temperature-related artefacts during CT acquisition.

2.2 | CT Technique

For CT evaluation, sequential transverse, dorsal and sagittal CT images were acquired using a 16-slice helical CT scanner (Aquilion Lightning, Canon Medical System, Tokyo, Japan). The birds were placed symmetrically in dorsal recumbency on the scanner table with a craniocaudal orientation. A standard protocol was followed, applying the following parameters: 100 kVp, 90 mA, 512 × 512 acquisition matrix, 2550 × 550 fields of view, a pitch of 0.94, and a gantry rotation time of 1.5. The obtained images had a slice thickness of 0.6 mm. To enhance the visualization of various anatomical structures in the CT images, different CT window settings were used by adjusting the window widths (WWs) and window levels (WLs): a bone window setting (WW = 1500; WL = 300), and a lung window setting (WW = 1400; WL = −500). No significant differences in CT density or anatomical structures were observed in the heads of the avian specimens included in this study. All images were analyzed using the DICOM viewer OsiriX MD 13.0.2 (Pixmeo, Bernex, Switzerland). Subsequently, the DICOM files were postprocessed to generate three-dimensional reconstructions, including maximum intensity projection (MIP) and volume-rendered (VR) reconstructed images of the heads.

2.3 | Anatomical Sections

After the CT study, the bird specimens were embedded in a foam and stored at −80°C until completely frozen. Subsequently, the three carcasses were transversely sectioned from the beak to the eyeballs with an electric band saw, obtaining sequential 1 cm thick slices. Transverse anatomical slices were performed at consistent intervals using the CT images as a spatial reference. Each section was thoroughly rinsed with water to remove debris, eliminating any artefacts using Adson forceps. Finally, both sides of each slice were photographed to accurately correlate the anatomical structures with the corresponding CT images.

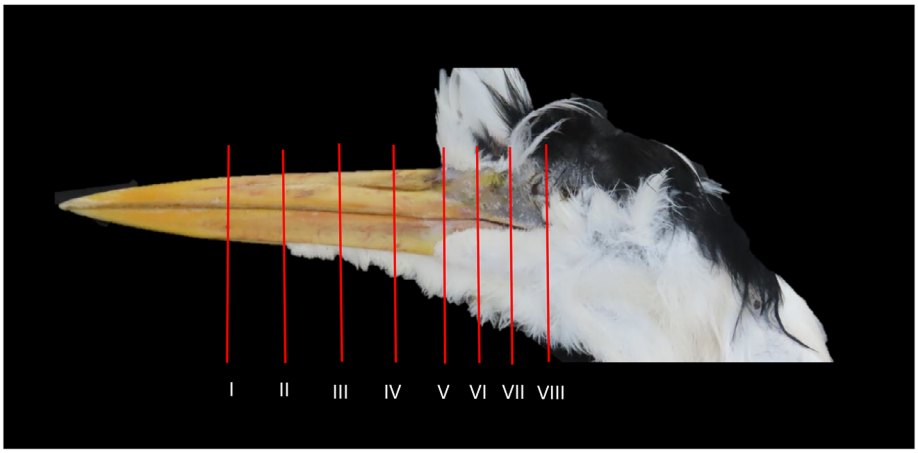

FIGURE 1 | Anatomical (labelled with red lines) image corresponding to the approximate levels of the transverse slices of the grey heron's (*Ardea cinerea*) nasal cavity.

2.4 | Anatomic Evaluation

To accurately identify and label the cross-sectional anatomy in correlation with the corresponding CT images, key anatomical landmarks—such as the nasal septum, conchae, infraorbital sinus recesses and surrounding cranial bones—were used to match each anatomical section with its corresponding CT image. The matching process was further validated by comparing the shape, orientation and relative position of these structures in both modalities.

In addition, we consulted a range of anatomical sources, including textbooks, skull preparations and key references describing avian anatomy in both aquatic and non-aquatic species (Codner et al. 1993; Boisteau and Marion 2007; Lauridsen et al. 2011; Orosz and Lichtenberger 2011; Bavdek et al. 2017; Casteleyn et al. 2018; Madkour 2019; Kvarnemo et al. 2025). These resources greatly enriched our comprehension and ability to interpret the anatomy of the grey heron's nasal cavity. Anatomical terminology follows the Nomina Anatomica Avium (Baumel et al. 1993).

3 | Results

A set of figures depicting the anatomical structures of the grey heron's nasal cavity and related formations is presented (Figures 1–12). Figure 1 is a lateral image of a grey heron's head, where each numbered line corresponds to the approximate levels of the anatomical and transverse CT sections shown in the following figures (Figures 2–9). These figures include three types of images: (A) an anatomical cross-section, (B) a CT scan using the bone window setting, and (C) a CT scan using the lung window setting. The sequence of images progresses in a rostrocaudal direction, starting at the beak and continuing to the orbital fossa. Figure 10 depicts a dorsal CT image at different levels, displaying pivotal formations comprising the nasal cavity and related structures. Finally, Figures 11 and 12 show some CT reconstructions using pulmonary and soft-tissue algorithm and OsiriX software to aid in the identification of structures and to compare different perspectives.

3.1 | Anatomical Sections

Cross-sectional anatomical analysis allowed precise identification of the clinically relevant structures of the nasal cavity, from the nostrils to the choanal cleft. As in other avian species, the nostrils were located at the base of the beak (Figure 5A). The nasal septum, clearly visualized along multiple transverse levels (Figures 5A and 8A), divided the left and right nasal passages and contributed to maintaining the structural rigidity of the elongated beak.

The floor of the nasal cavity was supported rostrally by the palatine processes of the maxilla, and more caudally by the thin palatine bone (Figures 8A and 9A) and the vomer (Figures 7A and 8A). The roof was formed by the premaxillary (Figures 2A–4A), nasal (Figures 5A–7A) and maxillary bones (Figures 2A–6A), and more caudally by the frontal (Figure 8A and Figure 9A) and lacrimal bones (Figure 8A). The nasal bone also exhibited a distinct nasal process and clear pneumatization (Figures 5A–7A), which likely contributes to cranial lightening, an adaptation commonly observed in long-beaked wading birds. Other bones were distinguishable throughout the cross-sections, including the mandible (Figures 2A–9A), jugal (Figures 7A–9A) and pterygoid bones (Figure 9A).

The nasal cavity displayed a cone-shaped configuration, with three conchae forming its caudal portion: the rostral (Figure 4A), middle (Figures 5A and 6A) and caudal nasal conchae (Figures 7A and 8A). The rostral concha had a smooth medial surface and likely participated in initial airflow direction. The middle nasal concha, the largest in size, appeared immediately caudal to the rostral one. It offered an extensive mucosal surface, supporting its expected roles in air humidification, thermoregulation and possibly in optimizing laminar airflow. The caudal nasal concha, located rostrally to the eye, connected to the infraorbital sinus (Figures 5A–8A) rather than to the nasal lumen, suggesting a functional relationship between sinus aeration and pressure modulation.

This sinus occupied a triangular space within the maxilla, with its opening identifiable in Figures 3A and 4A. Its rostral diverticulum

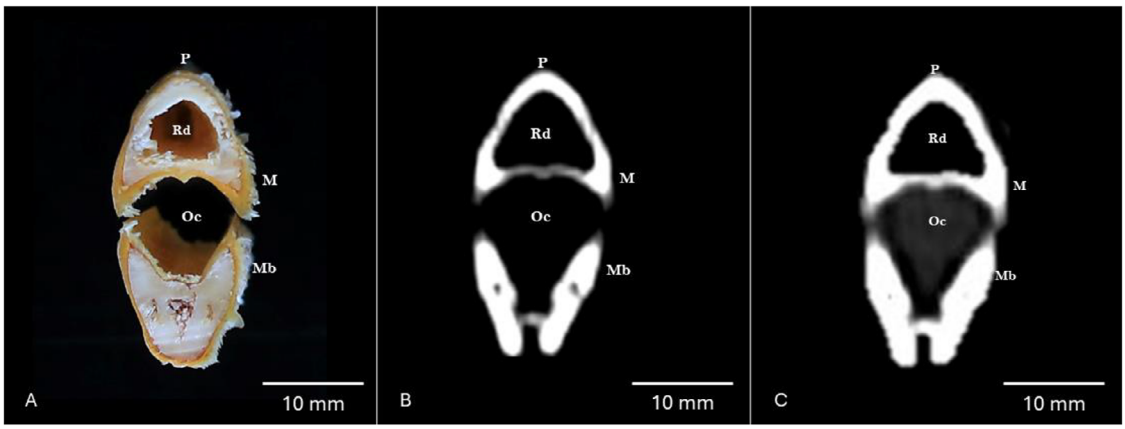

FIGURE 2 | Transverse cross-section (A), bone window (B), and pulmonary window (C) CT images at the level of line I in Figure 1. M: maxillary bone; Mb: mandible; Oc: oral cavity; P: premaxillary bone; Rd: rostral diverticulum of the infraorbital sinus.

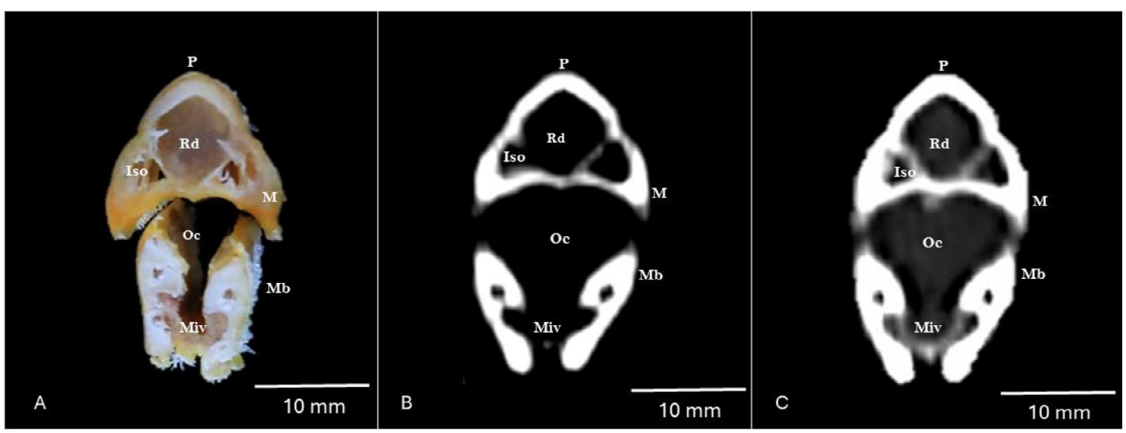

FIGURE 3 | Transverse cross-section (A), bone window (B), and pulmonary window (C) CT images at the level of line II in Figure 1. Iso: infraorbital sinus opening; M: maxillary bone; Mb: mandible; Miv: ventral intermandibular muscle; Oc: oral cavity; P: premaxillary bone; Rd: rostral diverticulum of the infraorbital sinus.

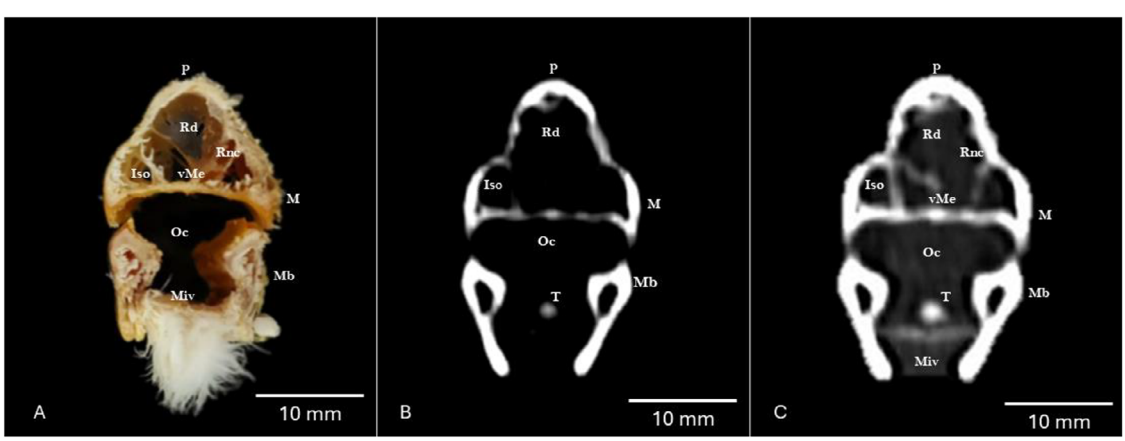

FIGURE 4 | Transverse cross-section (A), bone window (B), and pulmonary window (C) CT images at the level of line III in Figure 1. Iso: infraorbital sinus opening; M: maxillary bone; Mb: mandible; Miv: ventral intermandibular muscle; Oc: oral cavity; P: premaxillary bone; Rd: rostral diverticulum of the infraorbital sinus; Rnc: rostral nasal concha; T: tongue; vMe: ventral nasal meatus.

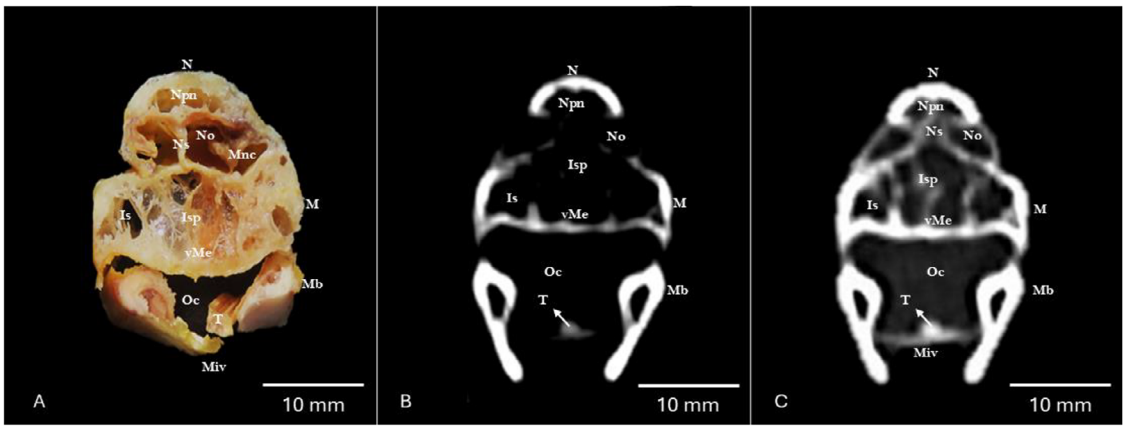

FIGURE 5 | Transverse cross-section (A), bone window (B), and pulmonary window (C) CT images at the level of line IV in Figure 1. Is: infraorbital sinus; Isp: infraorbital sinus pneumatization; M: maxillary bone; Mb: mandible; Miv: ventral intermandibular muscle; Mnc: middle nasal concha; N: nasal bone; No: nostrils; Npn: nasal bone pneumatization; Ns: nasal septum; Oc: oral cavity; T: tongue; vMe: ventral nasal meatus.

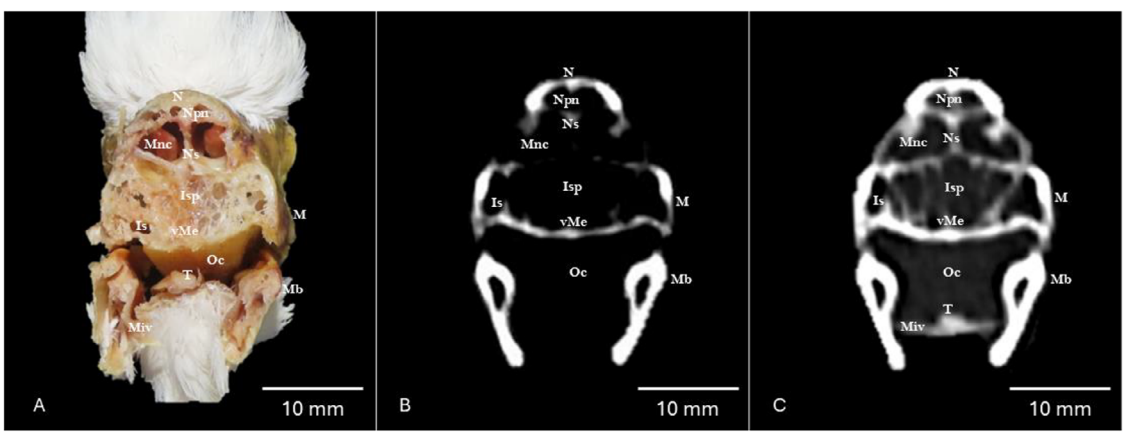

FIGURE 6 | Transverse cross-section (A), bone window (B), and pulmonary window (C) CT images at the level of line V in Figure 1. Is: infraorbital sinus; Isp: infraorbital sinus pneumatization; M: maxillary bone; Mb: mandible; Miv: ventral intermandibular muscle; Mnc: middle nasal concha; N: nasal bone; Ns: nasal septum; Npn: nasal bone pneumatization; Oc: oral cavity; T: tongue; vMe: ventral nasal meatus.

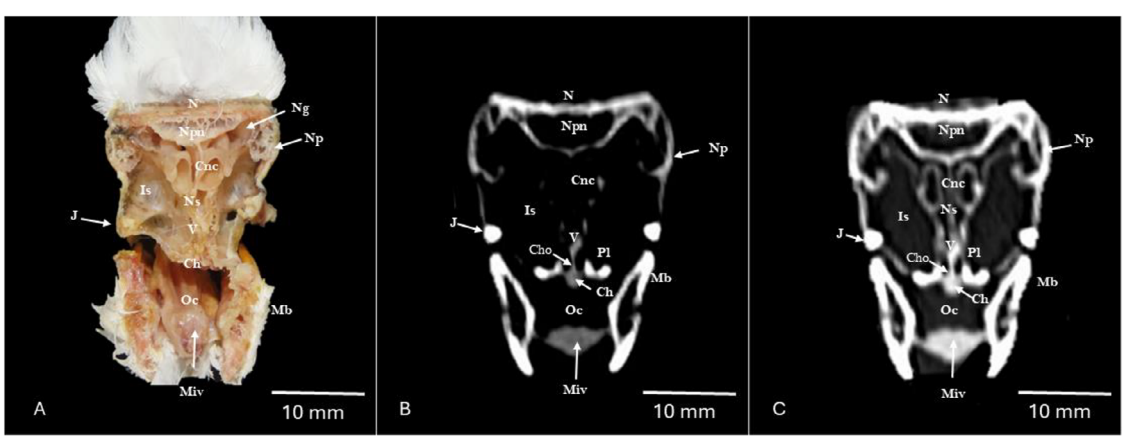

FIGURE 7 | Transverse cross-section (A), bone window (B), and pulmonary window (C) CT images at the level of line VI in Figure 1. Ch: choanal cleft; Cho: choanal opening; Cnc: caudal nasal concha; Is: infraorbital sinus; J: jugal bone; Mb: mandible; Miv: ventral intermandibular muscle; N: nasal bone; Ng: nasal gland; Np: nasal process; Npn: nasal bone pneumatization; Ns: nasal septum; Oc: oral cavity; Pl: palatine bone; V: vomer.

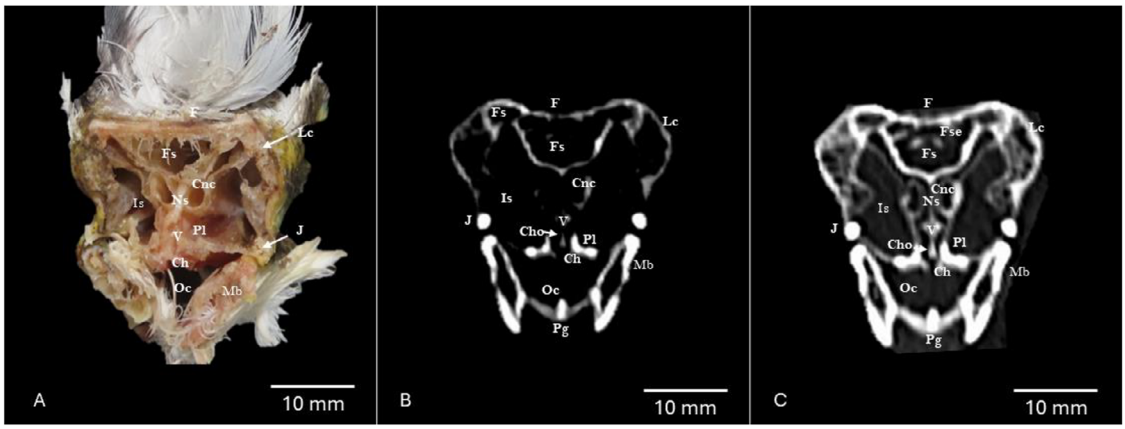

FIGURE 8 | Transverse cross-section (A), bone window (B), and pulmonary window (C) CT images at the level of line VII in *Figure 1*. Ch: choanal cleft; Cho: choanal opening; Cnc: caudal nasal concha; F: frontal bone; Fs: frontal sinus; Fse: frontal septum; Is: infraorbital sinus; J: jugal bone; Lc: lacrimal bone; Mb: Mandible; Ns: Nasal septum; Oc: Oral cavity; Pg: paraglossum; Pl: palatine bone; V: vomer.

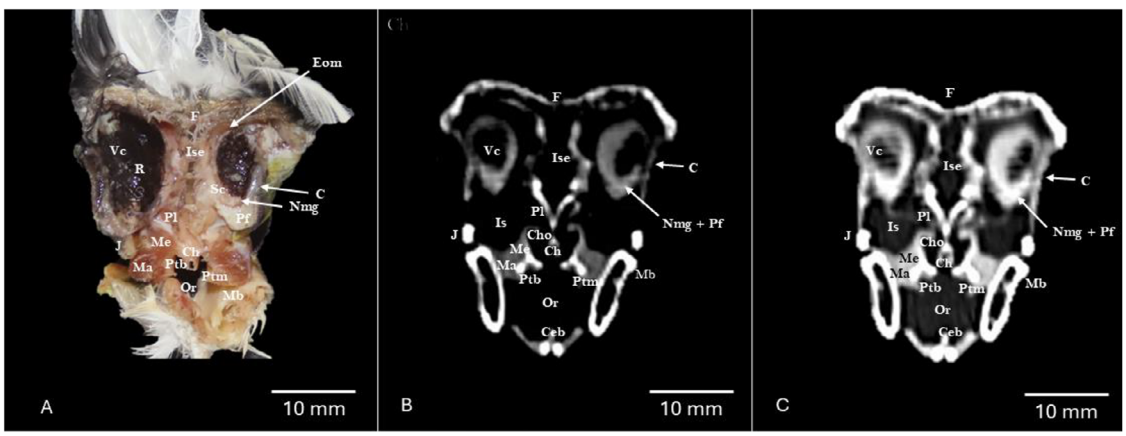

FIGURE 9 | Transverse cross-section (A), bone window (B), and pulmonary window (C) CT images at the level of line VIII in Figure 1. C: cornea; Ceb: ceratobranchiale; Ch: choanal cleft; Cho: choanal opening; Eom: extraocular muscle (superior oblique muscle); F: frontal bone; Ise: interorbital septum; J: jugal bone; Ma: mandibular adductor externus ventralis muscle; Mb: Mandible; Me: ethmomandibular muscle; Nmg: nictitating membrane gland; Or: Oropharynx; Pf: periorbital fat; Pl: palatine bone; Ptb: pterygoid bone; Ptm: pterygoid muscle; R: retina; Sc: sclera; Vc: vitreous chamber.

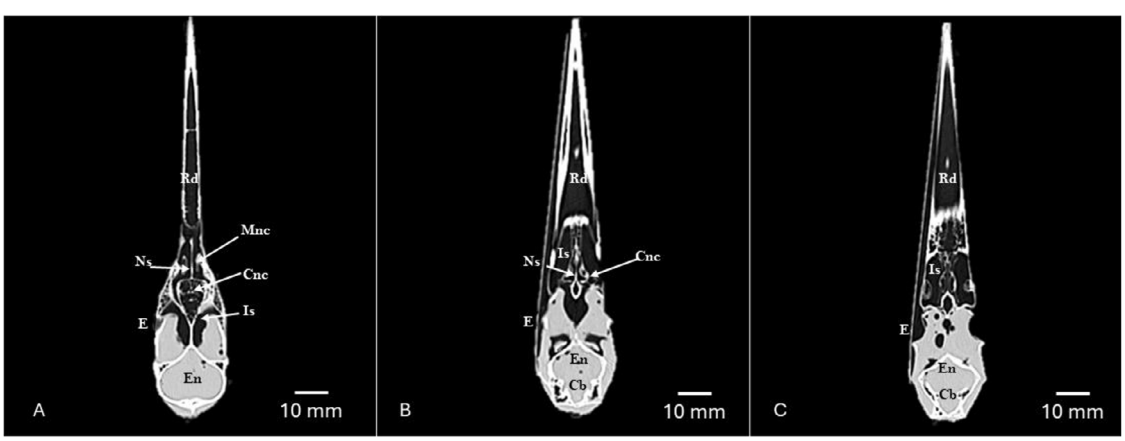

FIGURE 10 | Dorsal view of a pulmonary and soft-tissue algorithm CT images of the grey heron's head at different levels. Cb: cerebellum; Cnc: caudal nasal concha; E: eyeball; En: cerebrum; Is: infraorbital sinus; Mnc: medial nasal concha; Ns: nasal septum; Rd: rostral diverticulum of the infraorbital sinus.

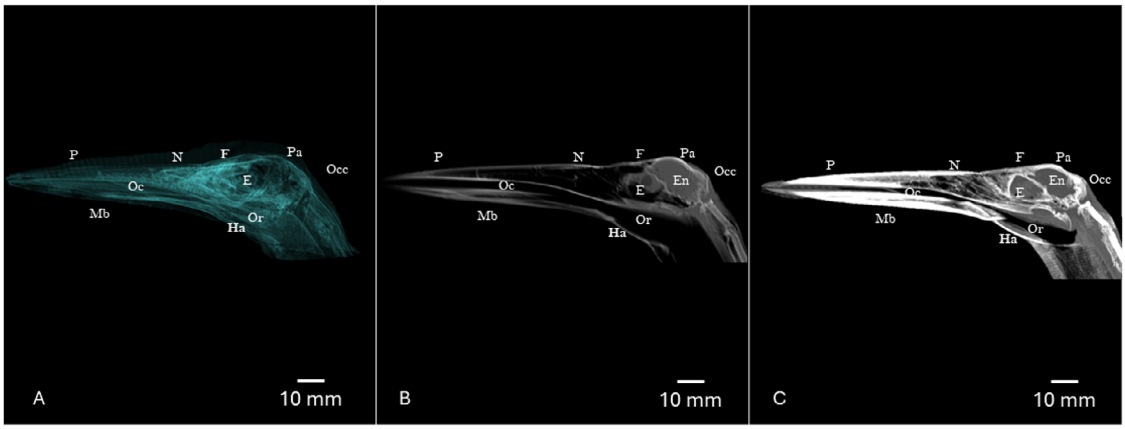

FIGURE 11 | Sagittal view using OsiriX MIP reconstructed CT image (A), bone window (B), and pulmonary window (C) CT images of the grey heron's head isolating bones and air spaces. E: eye (orbit); En: cerebrum; F: frontal bone; Ha: hyobranchial apparatus; Mb: mandible; N: nasal bone; Oc: oral cavity; Occ: occipital bone; Or: oropharynx; P: premaxillary bone; Pa: parietal bone.

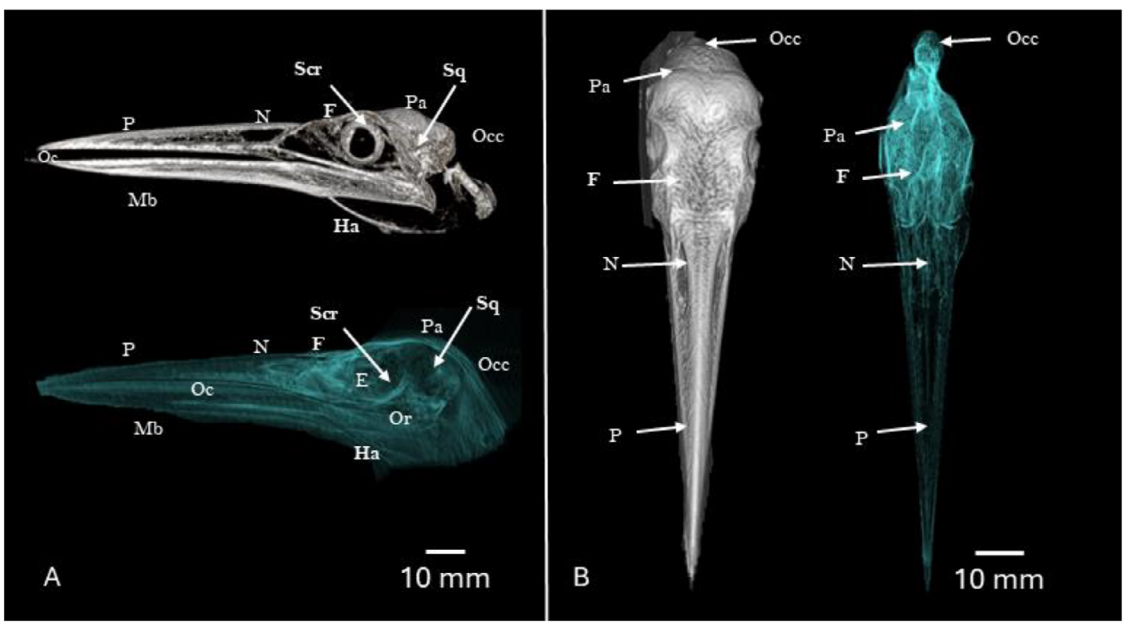

FIGURE 12 | Lateral view (A) and dorsal view (B) using OsiriX MIP reconstructed and volume rendering (VR) CT images of the grey heron's head, isolating bones and air spaces. E: eye (orbit); F: frontal bone; Ha: hyobranchial apparatus; Mb: mandible; N: nasal bone; Oc: oral cavity; Occ: occipital bone; Or: oropharynx; P: premaxillary bone; Pa: parietal bone; Scr: scleral ring; Sq: squamosal bone.

(Figures 2A–4A) extended rostroventrally toward the eye. This sinus exhibited pneumatization characterized by a trabeculated pattern across multiple segments (Figures 5A and 6A), contributing to cranial weight reduction and potentially influencing airflow dynamics around the orbit. The interorbital septum was also visible at the midline between the orbits (Figure 9A). The nasal meatuses (Figures 4A–6A) were clearly delineated, although the nasolacrimal duct could not be fully visualized due to its minute size; its expected course between the middle nasal concha and the dorsal aspect of the sinus was inferred from adjacent structures.

Cross-sections also revealed key formations of the oral cavity (Figures 2A–8A), including the tongue (Figures 5A and 6A) and oropharynx (Figure 9A). The choanal cleft (Figures 7A–9A), connected the nasal cavity to the oral cavity, and displayed a slit-like shape rostrally and a triangular configuration caudally. Its elongated morphology may facilitate rapid clearance of water or debris during feeding, particularly in aquatic foraging contexts. It was positioned between the palatine bones and bounded dorsally by the vomer and nasal septum.

Soft tissue structures resembling the nasal gland were discernible (Figure 7A), located medially to the lacrimal bone and rostrally adjacent to the nasal and frontal bones. Although small and poorly developed, this gland may contribute to humidity regulation and minor secretion into the nasal vestibule. Other

notable elements included the gland of the nictitating membrane (Figure 9A).

Muscular structures, including the ventral intermandibular muscle (Figures 3A–7A), as well as the pterygoid, ethmomandibular and mandibular adductor externus ventralis muscles (Figure 9A), were distinctly defined, reflecting their role in jaw support and fine motor control during prey capture. Extraocular muscles surrounding the eyeball, along with the surrounding periorbital fat, were distinctly visualized (Figure 9A). Additionally, cross-sections facilitated the observation of various orbital components, such as the vitreous chamber, retina, sclera and cornea (Figure 9A).

3.2 | Computed Tomography

No significant differences were observed among the three herons. CT imaging consistently allowed identification of the major sinonasal and cranial structures, with bones displaying marked hyperattenuation and soft tissues and air-filled cavities showing hypoattenuation across both pulmonary and bone windows.

The rostral diverticulum of the infraorbital sinus appeared as a hypoattenuating cavity extending within the premaxillary bone toward the nasal septum (Figures 2B,C, 3B,C, 4B,C and 10A–C). The infraorbital sinus itself was also hypoattenuating and increased progressively in size in the caudal direction (Figures 3B,C–8B,C and 10 A–C). Comparable attenuation was observed in the nostrils (Figure 5 B,C).

Within the oral cavity, the tongue was moderately hyperattenuating (Figures 4B,C, 5B,C and 6C), and the ventral intermandibular musculature was visible ventral to the oral structures (Figures 3B,C, 4C, 5C, 6C and 7B,C). The ventral nasal meatus appeared as a hypoattenuated space between these structures (Figures 4C, 5B,C and 6B,C). The rostral, middle and caudal nasal conchae could be distinguished, most clearly in the pulmonary window (Figures 4C, 6B,C, 7B,C, 8B,C and 10A,B). In addition, the elongated choanal cleft and its opening were also clearly visible (Figures 7B,C–9B,C).

Cranial musculature, including the mandibular adductor externus ventralis and pterygoid muscle, was identified (Figure 9B,C). Ocular structures were well defined, including the vitreous chamber, cornea, nictitating membrane gland and surrounding periorbital fat (Figure 9B,C). CT imaging also provided clear identification of major skull bones, such as the premaxillary (Figures 2B,C–4B,C), maxillary (Figures 2B,C–6B,C), mandible (Figures 2B,C–9B,C), nasal (Figures 5B,C–7B,C), jugal and palatine (Figures 7B,C–9B,C), vomer (Figures 7B,C and 8B,C), pterygoid (Figure 9B,C) and frontal bone (Figures 8B,C and 9B,C), which appeared hyperattenuated in both pulmonary and bone window settings.

Three-dimensional reconstructions generated using OsiriX software, together with sagittal and dorsal reformatted CT images, offered enhanced spatial context (Figures 10–12). Among the cranial bones identified, we included the squamosal bone (Figure 12A), as well as the premaxillary, nasal, frontal, parietal and occipital bones—including its basioccipital, exoccipital and supraoccipital portions—along with the mandible and the epibranchial bone of the hyobranchial apparatus (Figures 11A–C and 12A). In addition, other structures such as the cerebrum (Figures 10A–C and 11B,C), cerebellum (Figure 10B,C), eye (Figures 10A–C,11A–C and 12A), the sclerotic ring (Figure 12A), oral cavity and oropharynx (Figures 11A–C and 12A) were clearly delineated.

4 | Discussion

Herons are widely distributed wading birds that inhabit a broad range of aquatic and semi-aquatic ecosystems worldwide. Despite their adaptability, they remain vulnerable to various natural and anthropogenic threats. Climatic phenomena such as El Niño have been associated with increased flooding events, resulting in the destruction of nests and reduced breeding success (Fasola et al. 2009; Sovrano et al. 2019). Additionally, stagnant, warm waters where grey herons commonly reside can promote the proliferation of *Clostridium botulinum* (Diario de Gran Canaria 2020). Other anthropogenic hazards include collisions with electrical wires and secondary poisoning from rodenticides accumulated through the food chain (Ogórek et al. 2022).

Recent findings suggest a modest recovery in grey heron populations, likely owing to their ecological plasticity and widespread distribution (Boisteau and Marion 2007; Fasola et al. 2009). Nevertheless, the environmental pressure and energetic demands associated with an aquatic lifestyle highlight the importance of understanding their cranial anatomy, since specific anatomical adaptations may play a crucial role in their ability to regulate temperature, pressure, and respiration in fluctuating and often challenging habitats. In this context, the present anatomical–CT atlas provides clinically relevant information that may assist veterinarians working with free-ranging or rehabilitated herons. Specifically, species-specific anatomical references are essential for interpreting complex structures such as the conchal system, infraorbital sinus, septal sinus and choanal cleft, which commonly present with inflammatory, infectious or traumatic lesions in clinical practice. The combined use of CT imaging and anatomical sections in this study offers a practical diagnostic framework that may help distinguish normal anatomical pneumatization from soft-tissue opacification, foreign bodies, or sinus fluid accumulation in affected birds. Such references are especially valuable given the lack of standardized imaging descriptions for long-beaked wading species.

One such feature is the infraorbital sinus, a structure that differs markedly from its mammalian counterparts. The different CT windows and planes used in this study were quite helpful in identifying the complex arrangement of interconnected cavities extending from the rostral nasal concha to the ventral aspect of the eyeball. Although its function remains partially understood, previous studies on species such as Cory's shearwater, yellow-legged gull and ostrich suggest potential roles in airflow direction and pressure regulation (Yokosuka et al. 2009; Porter and Witmer 2016; Bavdek et al. 2017; Aref et al. 2024; Morales-Espino, Fumero-Hernández, et al. 2024; Jaber et al.,2025). Given the clinical frequency of sinusitis and orbital involvement in aquatic birds admitted to rehabilitation centres, this atlas may help clinicians

better identify pathological alterations affecting this sinus system (Montesdeoca et al. 2017).

Although the grey heron inhabits freshwater and brackish environments, it does not forage in fully marine waters. Consequently, it lacks the specialized nasal glands for salt excretion, as demonstrated using anatomical sections and CT imaging (Dunson et al. 1971; Shuttleworth et al. 1987; Franklin and Grigg 1993; Babonis and Evans 2011; Grosell et al. 2020; Morales-Espino, Fumero-Hernández, et al. 2024; Jaber et al. 2025). In our study, we identified only a small, underdeveloped glandular structure similar to the nasal gland, consistent with its limited osmoregulatory needs. Further histological work will be required to determine whether this gland shows any functional secretory activity.

Regarding the nasal septum, it exhibited a general structural layout similar to other avian and mammalian species (Basha et al. 2022), although in the grey heron, a distinct caudal extension was observed. The integration of anatomical slices with CT imaging enabled accurate identification of the septal sinus, which appeared as a clearly delineated cavity—a feature not uniformly present across avian taxa (Burk 1992; Aref et al. 2024; Martínez et al. 2024a, 2024b; Kazemi et al. 2025). From a clinical standpoint, understanding the limits of the septum is essential for interpreting unilateral versus bilateral nasal lesions in diagnostic imaging.

Within the nasal cavity, the nasal conchae followed a rostrocaudal arrangement, rendering traditional mammalian descriptors (dorsal, middle and ventral) less applicable. The largest and most complex structure was the middle nasal concha, which likely plays a role in humidification, airflow control and olfaction, aligning with observations in various aquatic and land bird species such as the cockatiel, ostrich, parrots, pigeon and puffin (Stańczyk et al. 2018; Jones et al. 2019; Fumero-Hernández et al. 2023; Aref et al. 2024; Kazemi et al. 2025). The combined anatomical–CT approach greatly improved visualization of regions that were poorly defined in CT alone, reinforcing the atlas's diagnostic utility.

Olfactory epithelium in birds, including the grey heron, is primarily located in the caudal nasal conchae. Although less developed than in mammals, avian olfaction supports behaviours like foraging, navigation and social interaction, with interspecies variability (Hadden et al. 2022). Our imaging revealed the relationship between the caudal nasal concha and the infraorbital sinus, offering insights into the structural organization of this sensory system (Basha et al. 2022).

The choana displayed an elongated configuration, more similar to that described in certain seabirds (Morales-Espino, Fumero-Hernández, et al. 2024) than to terrestrial species. This feature may facilitate efficient conduction between the nasal cavity and the oropharynx, and it also provides a practical endoscopic access site for clinical diagnostics (Sandoval 2000; Mahmoud et al. 2018).

The vomeronasal organ is a fundamental chemosensory structure, involved in detecting pheromones and predator odours. In reptiles, it triggers defensive behaviours and assists in prey tracking, while in mammals, it mediates responses to predator scents. Although a rudimentary form appears during embryonic development in birds, it regresses before maturity, rendering it vestigial rather than functional (Papes et al. 2010). This differs from some aquatic and terrestrial vertebrates, where the organ is retained and plays important ecological roles (Casteleyn et al. 2018). The presence of the vomer bone, observed in our specimens, reflects the evolutionary legacy of this system, offering structural support within the nasal cavity despite the absence of a functional vomeronasal organ.

A major limitation of this study is that all specimens were juveniles. Ontogenetic changes may influence several cranial structures. In birds and mammals, sinus pneumatization, conchal definition and degree of ossification typically increase with age, potentially altering the relative size and thickness of some structures (Lauridsen et al. 2011). The presence of down feathers, which aid in thermoregulation, emphasizes their early developmental stage. Since the avian nasal cavity contributes to air humidification, filtration, water conservation and temperature regulation (Geist 2000; Casteleyn et al. 2018; Mahmoud et al. 2018), these findings may not fully represent the adult morphology. Additionally, the relatively small sample size reflects the limited availability of well-preserved grey heron specimens suitable for anatomical and CT-based analysis. Although such sample sizes are common in anatomical studies of wild avian species, studies including a larger number of specimens would be valuable to further confirm and expand the anatomical observations described here. Comparative analyses between juvenile and adult specimens would also help establish age-related anatomical baselines.

In this study, CT slices were carefully selected to match anatomical cross-sections. Sequential transverse images allowed detailed visualization of the nasal cavity while preserving spatial consistency with the bony structures. We did not perform sagittal or dorsal anatomical sections due to the limited sample size and to prioritize accurate correspondence with transverse CT sections. As reported in previous work (Burk 1992), CT image quality improves with specimen size. This was evident in the grey heron, whose larger beak volume allowed for better CT definition compared to smaller avian species (Fumero-Hernández et al. 2023; Aref et al. 2024; Morales-Espino, Fumero-Hernández, et al. 2024; Kazemi et al. 2025). Nonetheless, image clarity was still constrained by the small overall volume and narrow height of the nasal region—measuring approximately 16 cm in length from the beak to the orbit, but only 1–3 cm in height along the rhamphotheca. As a result, structures like the ophthalmic branch of the trigeminal nerve—visualized in larger species or higher-resolution imaging (Wild and Zeigler 1996; Williams and Wild 2001)—were not identifiable. Notably, applying the lung window setting enhanced the visibility of soft tissues within the nasal cavity, proving valuable in delineating finer anatomical details. These difficulties could potentially be mitigated using micro-CT, which offers superior resolution in studies involving other exotic species. Despite its advantages, this remains largely inaccessible in routine veterinary practice due to its cost and technical demands, limiting its use to research centres or institutions with advanced imaging capabilities (Hadden et al. 2022). Nevertheless, the combination of CT scans and anatomical cross-sections allowed for the observation of the structural boundaries and configuration, which is essential for diagnostic purposes and may be applicable to other avian species.

Three-dimensional reconstruction software enhanced the anatomical assessment by providing a clearer visualization of the spatial relationships among the nasal cavity, infraorbital sinus and surrounding cranial bones, which may be difficult to fully appreciate using only sequential transverse CT slices. From a clinical perspective, this approach may improve the detection and interpretation of pathological alterations, including sinus fluid accumulation, soft-tissue thickening or structural displacement associated with trauma or inflammatory disease. Moreover, the ability to manipulate the reconstructed models allowed a better understanding of the extent and anatomical boundaries of the sinus system in relation to adjacent structures, which may assist veterinarians in planning diagnostic procedures or interpreting CT examinations in grey herons and other long-beaked avian species. Therefore, three-dimensional reconstructions complement conventional CT interpretation and represent a valuable tool for both clinical and educational applications (Mohamad et al. 2023; Martínez et al. 2024a).

5 | Conclusions

This investigation presents the first detailed anatomical description of the nasal cavity of the grey heron (*A. cinerea*), using CT images in transverse, sagittal and dorsal planes combined with anatomical cross-sections. The resulting images proved highly effective in identifying precise anatomical landmarks and spatial relationships within the nasal cavity. This information can assist veterinary clinicians in recognizing and diagnosing various pathological conditions affecting this region in herons. Additionally, the use of advanced imaging in anatomical research enhances education by allowing veterinary students and trainees to visualize complex structures without superimposition, thereby deepening their understanding of the avian rostral head. Ultimately, this species-specific anatomical knowledge strengthens diagnostic precision and supports the development of therapeutic strategies adapted to the unique features of the grey heron. Future studies, including a larger number of specimens and incorporating morphometric analyses, would be valuable to complement the descriptive findings presented here and to establish quantitative anatomical references for this species.

Author Contributions

Natalia Roldán-medina: investigation, writing – original draft, methodology, visualization, writing – review and editing, formal analysis. **José Raduan Jaber**: methodology, visualization, investigation, writing – original draft, writing – review and editing, formal analysis. **Manuel Morales**: resources, methodology. **Pablo Paz-oliva**: investigation, writing – review and editing, formal analysis, methodology. **Alejandro Morales-espino**: investigation. **Álvaro Ros**: formal analysis, writing – review and editing, methodology, investigation. **Francisco Suárez-cabrera**: resources, writing – review and editing. **Carlos Melián**: investigation, formal analysis, methodology. **Esteban Pérez**: investigation, formal analysis, methodology.

Acknowledgement

In loving memory of Alvaro Domingo and Honorio Rodriguez Garcia. We also thank Ayesh Mohamad, Carmen Mingot, Emilia Mingot, Concha Mingot, Nicolas Aquino, Marisa Mohamad and Jamal Jaber for their support and constructive comments. Moreover, we also thank the important contribution made by José Luis Roldán, Zoraida Medina, Daniela Roldán, Zoraida González, Maria Teresa Roa and Julián Cuello, and the Centro de Recuperación de Fauna Silvestre 'La Tahonilla.'

Funding

The authors have nothing to report.

Ethics Statement

The authors confirm that the ethical policies of the journal, as noted on the journal's author guidelines page, have been adhered to, and the appropriate ethical review committee approval has been received. The US National Research Council's guidelines for the Care and Use of Laboratory Animals were followed.

Conflicts of Interest

The authors declare no conflicts of interest.

Data Availability Statement

The data that support the findings of this study are available at https://accedacris.ulpgc.es.

Peer Review

For transparency, the peer review documents associated with this article are available at https://doi.org/10.1002/vms3.70953.

References

Aref, M., M. A. E. Raouf, W. O. M. Youssef, et al. 2024. "Structural Investigations of the Normal Ostrich Head Using Anatomical Sections, Computed Tomography, and Magnetic Resonance Imaging." *Open Veterinary Journal* 14, no. 12: 3487. https://doi.org/10.5455/ovj.2024.v14.i12.32.

Arencibia, A., J. M. Vazquez, R. Jaber, et al. 2000. "Magnetic Resonance Imaging and Cross Sectional Anatomy of the Normal Equine Sinuses and Nasal Passages." *Veterinary Radiology & Ultrasound* 41, no. 4: 313–319. https://doi.org/10.1111/j.1740-8261.2000.tb02079.x.

Babonis, L. S., and D. H. Evans. 2011. "Morphological and Biochemical Evidence for the Evolution of Salt Glands in Snakes." *Comparative Biochemistry and Physiology Part a Molecular & Integrative Physiology* 160, no. 3: 400–411. https://doi.org/10.1016/j.cbpa.2011.07.008.

Basha, W., S. M. Farouk, and S. Hassan. 2022. "Anatomical, Histochemical and Surface Ultrastructural Characteristics of Cavum Nasi of the Common Quails (*Coturnix coturnix. Erlangeri*)." *Anatomia Histologia Embryologia* 51, no. 4: 468–476. https://doi.org/10.1111/ahe.12808.

Baumel, J. J., A. S. King, J. E. Breazile, H. E. Evans, and J. C. Vanden Berge. 1993. *Handbook of Avian Anatomy: Nomina Anatomica Avium*. 2nd ed. Nuttall Ornithological Club.

Bavdek, S. V., Z. Golob, F. Janžekovič, C. S. Rutland, and V. Kubale. 2017. "Skull of the Grey Heron (*Ardea cinerea*): Detailed Investigation of the Orbital Region." *Anatomia Histologia Embryologia* 46, no. 6: 552–557. https://doi.org/10.1111/ahe.12308.

Boisteau, B., and L. Marion. 2007. "Habitat Use by the Grey Heron (*Ardea cinerea*) in Eastern France." *Comptes Rendus Biologies* 330, no. 8: 629–634. https://doi.org/10.1016/j.crvi.2007.05.006.

Burk, R. L. 1992. "Computed Tomographic Anatomy of the Canine Nasal Passages." *Veterinary Radiology & Ultrasound* 33, no. 3: 170–176. https://doi.org/10.1111/j.1740-8261.1992.tb01440.x.

Cardarelli, E., M. Fasola, A. Martinoli, and D. Pellitteri-Rosa. 2017. "Long-Term Changes in Food Intake by Grey Herons (*Ardea cinerea*), Black-Crowned Night-Herons (*Nycticorax nycticorax*) and Little Egrets (*Egretta garzetta*) Foraging in Rice Fields in Italy." *Waterbirds* 40, no. 4: 344–352. https://doi.org/10.1675/063.040.0406.

Casteleyn, C., P. Cornillie, S. Van Cruchten, W. Van Den Broeck, C. Van Ginneken, and P. Simoens. 2018. "Anatomy of the Upper Respiratory Tract in Domestic Birds, With Emphasis on Vocalization." *Anatomia Histologia Embryologia* 47, no. 2: 100–109. https://doi.org/10.1111/ahe.12336.

Codner, E., A. Lurus, J. Miller, P. Gavin, and D. Barbee. 1993. "Comparison of Computed Tomography With Radiography as a Noninvasive Diagnostic Technique for Chronic Nasal Disease in Dogs." *Journal of the American Veterinary Medical Association* 202, no. 7: 1106–1110. https://pubmed.ncbi.nlm.nih.gov/8473224/.

De Rycke, L. M., J. H. Saunders, I. M. Gielen, H. J. Van Bree, and P. J. Simoens. 2003. "Magnetic Resonance Imaging, Computed Tomography, and Cross-Sectional Views of the Anatomy of Normal Nasal Cavities and Paranasal Sinuses in Mesaticephalic Dogs." *American Journal of Veterinary Research* 64, no. 9: 1093–1098. https://doi.org/10.2460/ajvr.2003.64.1093.

Dunson, W. A., R. K. Packer, and M. K. Dunson. 1971. "Sea Snakes: An Unusual Salt Gland Under the Tongue." *Science* 173, no. 3995: 437–441. https://doi.org/10.1126/science.173.3995.437.

Diario De Gran Canaria. "El Centro de Fauna Silvestre atiende a una garza real que llegó débil e inmóvil por botulismo." 2020. Published October 21. https://diariodegrancanaria.opennemas.com/articulo/gran-canaria/centro-fauna-silvestre-garza-real/20201021202431002067.html.

Fasola, M., D. Rubolini, E. Merli, E. Boncompagni, and U. Bressan. 2009. "Long-Term Trends of Heron and Egret Populations in Italy, and the Effects of Climate, Human-Induced Mortality, and Habitat on Population Dynamics." *Population Ecology* 52, no. 1: 59–72. https://doi.org/10.1007/s10144-009-0165-1.

Franklin, C. E., and G. C. Grigg. 1993. "Increased Vascularity of the Lingual Salt Glands of the Estuarine Crocodile, *Crocodylus porosus*, Kept in Hyperosmotic Salinity." *Journal of Morphology* 218, no. 2: 143–151. https://doi.org/10.1002/jmor.1052180204.

Fumero-Hernández, M., M. Encinoso, A. Melian, H. A. Nuez, D. Salman, and J. R. Jaber. 2023. "Cross Sectional Anatomy and Magnetic Resonance Imaging of the Juvenile Atlantic Puffin Head (Aves, Alcidae, *Fratercula arctica*)." *Animals* 13, no. 22: 3434. https://doi.org/10.3390/ani13223434.

Garrido, J. R., B. Molina, and J. C Del Moral. 2011. "Las Garzas en España: Población Reproductora e Invernante en 2010–2011 y Método de censo." In *Ministerio Para La Transición Ecológica y El Reto Demográfico*. SEO/BirdLife. https://www.miteco.gob.es/content/dam/miteco/es/biodiversidad/temas/inventarios-nacionales/38-garzas_tcm30-207952.pdf.

Geist, N. R. 2000. "Nasal Respiratory Turbinate Function in Birds." *Physiological and Biochemical Zoology* 73, no. 5: 581–589. https://doi.org/10.1086/317750.

Gibbs, C., J. G. Lane, and H. R. Denny. 1979. "Radiological Features of Intra-Nasal Lesions in the Dog: A Review of 100 Cases." *Journal of Small Animal Practice* 20, no. 9: 515–535. https://doi.org/10.1111/j.1748-5827.1979.tb06760.x.

Grosell, M., R. M. Heuer, N. C. Wu, et al. 2020. "Salt-Water Acclimation of the Estuarine Crocodile *Crocodylus porosus* Involves Enhanced Ion Transport Properties of the Urodaeum and Rectum." *Journal of Experimental Biology* 223, no. pt. 4: jeb210732. https://doi.org/10.1242/jeb.210732.

Hadden, P. W., W. C. Ober, D. A. Gerneke, et al. 2022. "Micro-CT Guided Illustration of the Head Anatomy of Penguins (Aves: Sphenisciformes: Spheniscidae)." *Journal of Morphology* 283, no. 6: 827–851. https://doi.org/10.1002/jmor.21476.

Jaber, J. R., M. Morales, A. Ros, et al. 2025. "Study of the Nasal Cavity of the Cadaveric Yellow-Legged Gull (*Larus michahellis atlantis*) through Anatomical Cross-Sections and Computed Tomography." *Animals* 15, no. 21: 3114. https://doi.org/10.3390/ani15213114.

Jones, M. E. H., D. J. Button, P. M. Barrett, and L. B. Porro. 2019. "Digital Dissection of the Head of the Rock Dove (*Columba livia*) Using Contrast-Enhanced Computed Tomography." *Zoological Letters* 5, no. 1: 17. https://doi.org/10.1186/s40851-019-0129-z.

Kazemi, S., M. Rezaei, S. Alizadeh, and M. Hosseinchi. 2025. "Computed Tomographic Anatomy of the Head in Cockatiel (*Nymphicus hollandicus*)." *Veterinary Medicine and Science* 11, no. 2: e70234. https://doi.org/10.1002/vms3.70234.

King, A. S., and J. McLelland. 1984. *Form and Function in Birds*. Academic Press.

Kvarnemo, C., A. Anderstedt, M. Strandh, and D. Blomqvist. 2025. "The Importance of Olfaction for Mixed Paternity in Birds." *Ecology and Evolution* 15, no. 1: e70863. https://doi.org/10.1002/ece3.70863.

Lauridsen, H., K. Hansen, T. Wang, et al. 2011. "Inside Out: Modern Imaging Techniques to Reveal Animal Anatomy." *PLoS ONE* 6, no. 3: e17879. https://doi.org/10.1371/journal.pone.0017879.

Madkour, F. 2019. "Anatomical Descriptions of the Nasal Cavity of the Aquatic and Non-Aquatic Birds." *SVU- International Journal of Veterinary Sciences* 2, no. 2: 101–110. https://doi.org/10.21608/svu.2019.14982.1022.

Mahmoud, F. A., A. G. Gadel-Rab, and N. A. Shawki. 2018. "Functional Morphological Study of the Choana in Different Bird Species." *Journal of Basic and Applied Zoology* 79, no. 1: 11. https://doi.org/10.1186/s41936-018-0026-6.

Martínez, E. D., A. A. Espinosa, M. S. Laguía, et al. 2024a. "The Bony Nasal Cavity and Paranasal Sinuses of Big Felids and Domestic Cat: A Study Using Anatomical Techniques, Computed Tomographic Images Reconstructed in Maximum-Intensity Projection, Volume Rendering and 3D Printing Models." *Animals* 14, no. 17: 2609. https://doi.org/10.3390/ani14172609.

Martínez, E. D., A. A. Espinosa, M. S. Laguía, et al. 2024b. "An Anatomical Study Using Computed Tomography, Magnetic Resonance Imaging, and Rhinoscopy of the Nasal Cavity of Domestic Cat (*Felis silvestris catus* L.) and Big Cats: Lion (*Panthera leo leo* L.), Leopard (*Panthera pardus kotiya* L.), and Cheetah (*Acinonyx jubatus jubatus* S.)." *Animals* 14, no. 8: 1172. https://doi.org/10.3390/ani14081172.

Mohamad, J. R. J., E. González-Rodríguez, A. Arencibia, S. Déniz; C. Carrascosa, and M. Encinoso. 2023. "Anatomical Description of Loggerhead Turtle (*Caretta caretta*) and Green Iguana (*Iguana iguana*) Skull by Three-Dimensional Computed Tomography Reconstruction and Maximum Intensity Projection Images." *Animals* 13: 621.

Montesdeoca, N., P. Calabuig, J. A. Corbera, J. E. Cooper, and J. Orós. 2017. "Causes of Morbidity and Mortality, and Rehabilitation Outcomes of Birds in Gran Canaria Island, Spain, Bird Study." 64, no. 4: 523–534. https://doi.org/10.1080/00063657.2017.1411464.

Morales-Espino, A., S. Déniz, P. Paz-Oliva, et al. 2024. "Cory's Shearwater (*Calonectris borealis*): Exploring Normal Head Anatomy Through Cross-Sectional Anatomy, Computed Tomography and Magnetic Resonance Imaging." *Animals* 14, no. 13: 1962. https://doi.org/10.3390/ani14131962.

Morales-Espino, A., M. Fumero-Hernández, F. Suárez-Cabrera, M. Encinoso, M. M. Conde-Felipe, and J. R. Jaber. 2024. "Computed Tomography Anatomy of the Juvenile Cory's Shearwater (*Calonectris borealis*) Normal Nasal Cavity." *Animals* 14, no. 20: 3015. https://doi.org/10.3390/ani14203015.

Ogórek, R., J. Borzęcka, K. Kłosińska, et al. 2022. "A Culture-Based Study of Micromycetes Isolated From the Urban Nests of Grey Heron (*Ardea cinerea*) in SW Poland." *Animals* 12, no. 6: 676. https://doi.org/10.3390/ani12060676.

Orosz, S. E., and M. Lichtenberger. 2011. "Avian Respiratory Distress: Etiology, Diagnosis, and Treatment." *Veterinary Clinics of North America Exotic Animal Practice* 14, no. 2: 241–255. https://doi.org/10.1016/j.cvex.2011.03.003.

Papes, F., D. W. Logan, and L. Stowers. 2010. "The Vomeronasal Organ Mediates Interspecies Defensive Behaviors Through Detection of Protein Pheromone Homologs." *Cell* 141, no. 4: 692–703. https://doi.org/10.1016/j.cell.2010.03.037.

Porter, W. R., and L. M. Witmer. 2016. "Avian Cephalic Vascular Anatomy, Sites of Thermal Exchange, and the Rete Ophthalmicum." *Anatomical Record* 299, no. 11: 1461–1486. https://doi.org/10.1002/ar.23375.

Sandoval, J. 2000. *Tratado de Anatomía Veterinaria: Cabeza y Sistemas viscerales: Vol. Tomo III*. Imprenta Sorles.

Schwarz, T., M. Sullivan, and K. Hartung. 2000. "Radiographic Detection of Defects of the Nasal Boundaries." *Veterinary Radiology & Ultrasound* 41, no. 3: 226–230. https://doi.org/10.1111/j.1740-8261.2000.tb01483.x.

Shuttleworth, T. J., J. L. Thompson, and W. H. Dantzler. 1987. "Potassium Secretion by Nasal Salt Glands of Desert Lizard *Sauromalus obesus*." *AJP Regulatory Integrative and Comparative Physiology* 253, no. 1: R83–R90. https://doi.org/10.1152/ajpregu.1987.253.1.r83.

Sovrano, L. V., A. H. Beltzer, S. A. Regner, et al. 2019. "Inusual Mortandad de Pichones y Juveniles de Garza Bruja *Nycticorax nycticorax*(Ardeidae) en una Nueva Colonia Nidificante en el centro de Argentina." *Caldasia* 41, no. 2: 257–267. https://doi.org/10.15446/caldasia.v41n2.71255.

Stańczyk, E. K., M. L. V. Gallego, M. Nowak, J. Hatt, P. R. Kircher, and I. Carrera. 2018. "3.0 Tesla Magnetic Resonance Imaging Anatomy of the Central Nervous System, Eye, and Inner Ear in Birds of Prey." *Veterinary Radiology & Ultrasound* 59, no. 6: 705–714. https://doi.org/10.1111/vru.12657.

Veladiano, I. A., T. Banzato, L. Bellini, A. Montani, S. Catania, and A. Zotti. 2016. "Computed Tomographic Anatomy of the Heads of Blue-and-Gold Macaws (*Ara ararauna*), African Grey Parrots (*Psittacus erithacus*), and Monk Parakeets (*Myiopsitta monachus*)." *American Journal of Veterinary Research* 77, no. 12: 1346–1356. https://doi.org/10.2460/ajvr.77.12.1346.

Wild, J. M., and H. P. Zeigler. 1996. "Central Projections and Somatotopic Organisation of Trigeminal Primary Afferents in Pigeon (*Columba livia*)." *Journal of Comparative Neurology* 368, no. 1: 136–152. https://doi.org/10.1002/(SICI)1096-9861(19960422)368:1%3C136::AID-CNE9%3E3.0.CO;2-4.

Williams, M. N., and J. Wild. 2001. "Trigeminal Innervated Iron-Containing Structures in the Beak of Homing Pigeons, and Other Birds." *Brain Research* 889, no. 1–2: 243–246. https://doi.org/10.1016/s0006-8993(00)03114-0.

Wilson, M., D. Mauragis, and C. R. Berry. 2014. "Small Animal Skull & Nasofacial Radiography, Including the Nasal Cavity & Frontal Sinuses: University of Florida." Today's Veterinary Practice, March. https://imaging.vetmed.ufl.edu/files/2016/06/Small-Animal-Skull-Nasofacial-Radiography-Including-the-Nasal-Cavity-Frontal-Sinuses.pdf.

Yokosuka, M., A. Hagiwara, T. R. Saito, et al. 2009. "Histological Properties of the Nasal Cavity and Olfactory Bulb of the Japanese Jungle Crow *Corvus macrorhynchos*." *Chemical Senses* 34, no. 7: 581–593. https://doi.org/10.1093/chemse/bjp040.